Sanchis Sánchez, MJ.; Carsí Rosique, M.; Gracia-Fernandez, C. (2017). Thermal and Dielectric Characterization of Multi-Walled Carbon NanotubesThermoplastic Polyurethanes Composites. Polymer Science Series A. 59(4):543-553. doi:10.1134/S0965545X17040083

Thermal and Dielectric Characterization of Multi-walled carbon nanotubes (MWCNTs)-Thermoplastic polyurethanes (TPU) Composites[1]

M. J. Sanchis[a*], M. Carsí[a,b], C. A. Gracia-Fernández[c]

[a]*Departamento de Termodinámica Aplicada, E.T.S.I.I., Instituto de Tecnología Eléctrica Universitat Politècnica de Valencia, 46022 Valencia, Spain*

[b]*Instituto de Automática e Informática Industrial, Universitat Politècnica de Valencia, 46022 Valencia, Spain*

[c]*TA Instruments-Waters Cromatografía, 20108 Alcobendas, Madrid, Spain*

*Corresponding author: M.J. Sanchis; Tel.: 0034963879327; email: jsanchis@ter.upv.es

Abstract

Multi-walled carbon nanotubes (MWCNTs)-Thermoplastic polyurethanes (TPU) composites were characterized by means of differential scanning calorimetry (DSC) and Dielectric Relaxation Spectroscopy (DRS). The DSC analysis shows the existence of two glass transition temperatures (T_g) linked to the soft and hard segment of TPU. The T_g associated with the soft segment decrease by increasing MWCNT content, while the T_g associated with the hard segments is not affected significantly by the MWCNT content. DRS analysis was used to analyze how the MWCNT content affects the electrical properties of the composites. The results of DRS showed a correlation between MWCNT content and the electrical properties of the material. Thus, it was observed that rising temperature and MWCNT content, both increased the dielectric permittivity and the loss factor. Otherwise, the presence of MWCNT produces an enhancement of charge carriers trapping, increasing the electrical conductivity. The conductivity process was analyzed by means of several functions as (i) complex impedance ($Z^*(\omega)$), (ii) dielectric conductivity ($\sigma'(\omega)$) and loss dielectric modulus ($M''(\omega)$). From the study of the MWCNT content effect on the conductivity behavior, it follows that there is an increase of several orders of magnitude of the conductivity value. The electrical conductivity of the composite was found to exhibit an insulator to conductor transition at a MWCNT critical content, i.e. the percolation threshold, near 6% wt. The activation energy values, associated with the conductive process, obtained by the different procedures are in good agreement. The lower activation energy

[1] MJS and MC acknowledge the financial support of the DGCYT through Grant MAT2015-63955-R

values observed for the high MWCNT contents can be rationalized if we consider that the mean distance between MWCNT decreases with increasing MWCNT content.

Keywords: Nanocomposites. Multi-walled carbon nanotubes. Thermoplastic polyurethanes. Differential Scanning Calorimetry. Conductivity.

INTRODUCTION

Over coming years, science applied to the study of materials will be oriented to the development of so-called nanomaterials (nanocomposites) [1-2]. Mainly, the great interest of the nanocomposites, lies in the easy improve of various properties of the original material (matrix) by adding small amounts of nanometric components, due to the high area/volume relationship thereof [3-5]. A large number of conductive composites have been prepared by addition of electrically conductive particles, such as metallic powder [6-7], graphite [8-9], carbon black (CB) [10-12] and carbon nanotubes (CNT) [13-14] above a critical concentration into an insulating resin. These materials, which consist of a main matrix typically polymeric, and one or various components added to nanometric level to this matrix, will be the focus of this paper.

One of the most versatile polymeric materials used as matrix, due to they can behave as elastomers, thermoplastics, or thermoset polymers depending on the different reactants and synthesis conditions selected, are the polyurethane family. Its versatility together with their peculiar behavior makes them suitable to a wide range of applications (foams, elastomers, coatings, sealants, and adhesives) [15-17]. Thermoplastic polyurethanes (TPU) are linear block copolymers formed by thermodynamically incompatible segments named as soft and hard domains. The soft segment provides high flexibility at room temperature, whereas the hard segment provides physical crosslink sites through strong intermolecular hydrogen bonding. Therefore, you might motorize their properties (morphological, physical, chemical, and mechanical) by changing your formulation and content of the hard segment, molecular structure of soft segment, and manufacturing conditions.

During the new century, CNT's are being considered as a promise filler materials for a whole host of applications due to their unique properties, such as high electrical and thermal conductivity and ultrahigh mechanical strength [18-19] combined with their low density and

high aspect ratios. So, their electrical conductivity is higher than copper, heat conductivity is higher than diamond and are stronger than steel. The basic CNT morphologies are single-walled carbon nanotubes (SWCNT) and multi-walled carbon nanotubes (MWCNT). In recent years, both CNT morphologies have been widely used in order to improve the electrical properties of the polymer matrix in composite materials [20]. Nevertheless, MWCNTs are substantially cheaper and easier to experimentally manipulate compared to SWCNTs. Additionally, the increased use of this filler material also is linked to the continued advancements in cost reduction of their production. For this reason, in recent years the MWCNTs have been widely used, as filler in composite systems, since possess unique physicochemical characteristics in order to improve the properties of the polymer matrix [21-22]. The widespread use of carbon nanotube (CNT)-composites justifies the relevance of the study and characterization of this type of materials.

In this regard, in this work we report on our study into how the Multi-walled carbon nanotubes (MWCNTs) content affects the thermal and conductive properties of TPU/MWCNT composites for application mainly in the field of electrical and electronics. Differential scanning calorimetry (DSC) and Broadband dielectric relaxation spectroscopy techniques were employed to study the thermal and conductive properties of the composites. Importantly, the present study will focus on the phenomenological description and interpretation of the conductivity behavior of TPU/*x*-MWCNT composites as a function of the MWCNT content, temperature and frequency.

Experimental section

Materials. Samples Preparation

TPU/x-MWNT nanocomposites were prepared by melt mixing method in an internal batch mixer. The matrix is a TPU consisting of 50 % by mass hard segment (Methylene diphenyl diisocyanate), 1,4 butanediol as a diol chain extender, and 50 % soft segment (polyethyleneglycol adipate) that was supplied by Lubrizol Advanced Materials Inc., ThermedicsTM Polymer Products, Ohio, USA. Multi walled carbon nanotubes (MWCNT) consisting of multiple rolled layers (concentric tubes) of graphite were provided by Helix Material Solutions, Inc. Richardson TX, USA. Purity is about 95 % according to manufacturer specifications (length is in the range from 0.5 to 40 μm and the specific surface area is in the range from 40 to 300 $m^2 g^{-1}$). The mixing of samples were carried out at temperature of 185 °C with a rotor speed of 100 rpm and mixing time of 8 min. TPU pellets and MWCNTs were dried before processing to remove the water content if any in the supplied materials at 80 º and 120 °C in a preheated vacuum oven for 6 and 24 hr,

respectively. A scheme of the chemical structure of the TPU is shown in Fig. 1. The nomenclature used for labelling the samples and the MWCNT content in the mixtures with TPU is summarized in Table 1.

Methods

Surface morphology of samples was obtained using an ultra-high resolution field-emission microscope (Zeiss Ultra-55FEGSEM) equipped with an in-lens detection system. To get higher resolution, low voltage need to be applied. By using collecting-efficient through-the-lens (In-lens for Zeiss) detector, the resolution at low voltage mode can reach at the nanometer level. Small pieces of sample were placed in the sample holder to study the sample surface. Since the sputter coating may affect the quality of SEM images of the nanofiller, the samples not were coated. The analysis was carried out at accelerating voltages of 5kV and 1kV.

Differential scanning calorimetry (DSC) scans were performed using a TA Instrument Q20 (USA) equipped with a refrigerated cooling system and nitrogen purge. Calibration was undertaken with indium according with manufacturer recommended procedures. About 5-7 mg of sample was sealed in an aluminum pan for every test. Thermal behavior was investigated by scanning the samples from -90 ºC to 230 °C at a heating rate of 20°C min^{-1}. A second run (to delete the thermal history) was used for the thermal characterization of the films. The midpoint of the heat capacity change has been chosen to represent the glass transition temperature, T_g.

The analysis of the electrical behavior of TPU/*x*-MWCNT composites was carried out using broadband dielectric relaxation spectroscopy (DRS). Isothermal relaxation spectra of TPU/*x*-MWCNT composites were collected by using a Novocontrol Impedance Spectrometer (Novocontrol Technologies GmbH&Co. KG Montabaur, Germany) consisting of an Alpha analyzer to carry out measurements from $5 \cdot 10^{-2}$ to $3 \cdot 10^{6}$ Hz. The measurements were carried out in inert N_2 atmosphere between -20 to 170 °C. The temperature was controlled by a nitrogen jet (QUATRO from Novocontrol) with a temperature error of 0.1 °C during every single sweep in frequency. Molded disc shaped samples of about 0.20 mm thickness and 20 mm diameter was used. The experimental uncertainty was better than 5% in all cases.

One of the best potential of the linear dielectric analysis is that impedance data allows the analysis of processes related to: (a) charges transport across the samples and (b) dipoles motions associated with local and cooperative micro-Brownian motions of the molecular

chains [23-25]. Under an alternating voltage $V(\omega)$, the current crossing a sample sandwiched between two parallel plane electrodes can be expressed as $V(\omega)/Z^*(\omega)$, where $Z^*(\omega)$ is the complex impedance. The charge transport across the sample often dominates the dielectric response of a material at high temperatures and low frequencies. The processes that contribute to the dielectric response under these conditions include the migration of mobile charge carriers across the medium (ohmic conduction or electronic conduction) and the trapping of charges at interfaces and boundaries (non-ohmic conduction or polarizations effects). The last processes are the result of (i) accumulation of charges at the electrode-sample interface, called "electrode polarization" (EP) and/or (ii) the separation of charges at internal phase boundaries referred to as Maxwell–Wagner–Sillars (MWS) polarization. MWS polarization is generally evident in non-homogenous materials like multiphase polymers, blends and colloids, crystalline or liquid crystalline polymers, composites, etc. and occurs across smaller size scales when comparing to the EP.

In order to carry out the characterization of the different processes the dielectric response can be analysed in terms of several functions: $Z^*(\omega)$, $\varepsilon^*(\omega)$, $\sigma^*(\omega)$, $M^*(\omega)$,.... Each of the above cited processes has specific features in the frequency and temperature dependence of the real and imaginary part of these functions. The dielectric permittivity and the conductivity are expressed, respectively, in terms of the impedance as $\varepsilon^*(\omega) = (l/A) \cdot (1/i\omega e_0 Z^*(\omega))$ and $\sigma^*(\omega) = (l/A) \cdot (1/Z^*(\omega))$ where *A* and *l* are, respectively, the area and thickness of the sample between electrodes, e_0 *(=8.854 pF/m)* is the dielectric permittivity of the empty space and $\omega = 2\pi f$ is the angular frequency of the electric field. Other alternative representation of the dielectric properties of the material is the complex electric modulus $M^*(\omega) = 1/\varepsilon^*(\omega)$. The use of the last representation is very interesting because allow us to emphasize the charge transport in the material [24, 26].

Results and discussion

Fig. 2 shows a FESEM micrographs for the TPU/*x*-MWCNT nanocomposites obtained from Zeiss Ultra In-lens detector at 5 kV with a working distance (WD) of 4 mm (a-d) and at 1kV with a WD of 3.3mm (e). As we can see clearly in Fig. 2a-d, the formation of interconnected nanotubes rises as increasing the MWCNT content. Furthermore, in Fig. 2e is displayed as the MWCNT aggregates are dispersed non-uniformly in the TPU matrix.

The DSC thermograms obtained for all the samples are plotted in Fig. 3, and the characteristic parameters are summarized in Table 1. In all thermograms two endothermic

processes about -16 º and 79 ºC, respectively, associated with glass transitions (T_g) of the soft and hard segments of the TPU are observed. Both T_g values underwent changes with filler content. In Table 1 are summarized, for the six samples tested, the DSC characteristic parameters values of both processes. With increasing conductive filler content a clear decrease in the T_g associated with the soft segment is observed. This behavior can be associated with the increase of the free volume, promoted by a low affinity between the filler and the polymer matrix. That is, the reinforcement acts ~~as a lubricant,~~ favoring the sliding of the molecular chains. On the other hand, for the T_g of the hard segments only slight changes are observed as the reinforcing material increases. Two T_g associated to different segments of the polyurethane matrix have been reported in other related materials [27]. The temperature range of both glass transitions related to the sample heterogeneity increases with the MWCNT content. The trend of the heat capacity jump value (Δc_p) at T_g with the conductive filler content is different for the process related to the soft and hard segments. Thus, for the soft segment process, this parameter decreases with increasing the MWCNT content is observed, whereas an increase is observed for the hard segment process.

Additionally, at temperatures around 90 ºC, a transition associated with the melting of crystalline hard segment appears. This process, which is widely distributed, ends around 130 ºC. Also during the cooling cycle, about 50/70 ºC a slight exothermic peak, associated with crystallization of the material, is observed.

Fig. 4 shows the frequency dependency of the complex dielectric permittivity at 120 ºC for all samples tested. All the isotherms exhibit similar patterns. Both, dielectric permittivity and the loss factor isotherms exhibit, at low frequency and high temperatures, a dominant conductivity contribution. Thus, conductive and interfacial conductivity processes mask these dipolar processes especially at high temperature and low frequency and even more so for samples with high amount of conductive filler content.

When the data are represented in log-log scale, the loss permittivity increases linearly with decreasing frequency with a negative slope, according to $log_{10}\varepsilon''_{cond} = log_{10}(\sigma/\varepsilon_0) - s \cdot log_{10}(\omega)$, where σ is the conductivity arising from charge transport as the liquid-electrode interface and s is a constant ($s \leq 1$). As an example, in Table 2 is summarized the fit results of the loss permittivity at 140 ºC. As we can see, the intercept of the straight, related to the conductivity of the sample, increase with the MWCNT content and the s constant is approximately 1 for all the samples.

In order to better visualization of dipolar and conductive processes [26] in Fig. 5 is showed a representation of experimental results in terms of the imaginary part of the complex dielectric modulus, $M^{"}(\omega)$, at 20 ºC and 120 ºC. The complex modulus was evaluated from the complex permittivity as follow, $M^{"}(\omega) = 1/\varepsilon^{*}(\omega)$. At 20 ºC almost two processes are observed, related in order increasing frequencies to the conductive and dipolar processes. The two processes are shifted to higher frequencies by increasing temperature and the frequency of maximum is slightly higher for samples with highest conductive filler content. Moreover, it appreciates that by increasing the MWCNT content: (i) the value of $M^{"}_{max}$ corresponding to the conductive process decreases and (ii) the overlapping between the conductive and dipolar processes increases.

For the two composites with higher MWCNT content, not good definition of the maximum of conductive process $\left(M^{"}_{max}\right)$ was obtained. For this reason, only the temperature dependence of the f_{max}, of the conductive process, for TPU and for the three composites with lower MWCNT content is shown in Fig. 6. According to our results, this dependence is Arrhenius type. The fit parameters at Arrhenius equation obtained by multiple regressions linear, E_a and ln f_0, are summarized in Table 3. As we can observe the addition of MWCNT filler produces a reduction in the activation energy, E_a.

It is interesting to analyze the frequency dependence of the ac conductivity, for the purpose of characterizing the conductive process. These values were evaluated from measurements of complex dielectric permittivity, $\sigma' = \sigma_{ac}(\omega) = i\omega\varepsilon_0\varepsilon''(\omega)$. As usual, at a constant temperature, the ac conductivity can be expressed by mean of the often called "the ac universal law", $\sigma_{ac}(\omega) = \sigma_{dc} + A\omega^n$ where σ_{dc} is the $\omega \to 0$ limiting value of $\sigma_{ac}(\omega)$ and *A* and *n* are parameters depending of the temperature [28, 29]. For pure TPU, the conductivity increases with increasing frequency, as expected for an insulator material, with a value at room temperature and 10^{-1} s^{-1} of about 3×10^{-10} S m^{-1}. Their value increases to ca 7×10^{-7} S m^{-1} at 120 ºC and 10^{-1} s^{-1}, i.e. three orders of magnitude. The isotherms in the low frequency region, exhibit a plateau, reflecting a frequency independent conductivity, i.e., dc conductivity, σ_{dc}. The covered frequency range by this plateau increases with temperature. . On the other hand, when frequency is raised, the main displacement of the charge carriers is reduced, and the conductivity appears to be proportional to the frequency following the law $\sigma_{ac}(\omega) \propto A\omega^n$ with $0 \le n \le 1$. An increase of σ_{dc} with rising temperature and MWCNT content was observed. Furthermore, for MWCNT content equal to 10wt%, a frequency-independent conductivity is obtained in all the experimental frequency/temperature range.

For a proper analysis of the MWCNT content effect in the conductive process, a double logarithmic plots of the frequency dependence of the real component of the complex conductivity at 120 ºC for TPU, pure polymer, and TPU/*x*-MWCNT composites are shown in Fig. 7**.** The conductivity exhibits a frequency dependence, which becomes stronger as the concentration of MWCNT decreases and as is expected the MWCNT inclusion produces an increase in the dc conductivity of the samples. Moreover, for samples with MWCNT content less or equal to 6%, the frequency dependence of $\sigma'(\omega)$ is nearly linear [$\sigma'(\omega) \sim \omega^s$] in the high frequency range. However, for MWCNT content equal or higher than 6%, a frequency independent conductivity is obtained in all the experimental frequency range. This behavior could be related to the occurrence of a highly interconnected filler network with almost the absence of electrical barriers. Additionally, we can also observe that the dc conductivity significantly increases for MWCNT content higher than 6%. This observation suggests that the critical filler content, i.e. the percolation threshold, should be near 6% for this particular TPU/*x*-MWCNT composites (see inset Fig. 7). The relatively high value of the percolation threshold obtained may be associated with the non-uniform distribution of MWCNT in the matrix and to a non-effective interaction of both constituents. This percolation threshold can be reduced with surface treatments to promote the connection between the matrix and the MWCNT [30-32].

Fig. 6b shows the values of dc conductivity as a function of the reciprocal of the absolute temperature. These values were estimated from the plateau at low frequencies of the σ′. As we can see, the dc conductivity is thermally activated and can be described by $\sigma_{dc} = \sigma_0 \cdot e^{-E_a^{\sigma}/RT}$. The conductivity activation energy and the pre-factor parameters of the samples under study are summarized in Table 3.

One attractive feature of dielectric spectroscopy lies in the direct correlation between the response of a real system and idealized model circuit composed of discrete electrical components (resistors and capacitors) [29]. The equivalent circuit modeling the complex impedance in the frequency domain is made up of a constant phase element of admittance $Y^*(\omega) = Y_0(j\omega)^a$ $(0 < a \leq 1)$ in parallel with a polarization resistance R_p. The impedance of the equivalent circuit is given by [33]

$$Z^*(\omega) = \frac{R_p}{1+(j\omega\tau)^a} \quad (1)$$

where $Y_0 R_p = \tau^a$, being τ a mean-relaxation time. For some systems, the Cole plots are skewed arcs along a nearly straight line at high frequencies, and $Z^*(\omega)$ is better expressed in terms of the Havriliak-Negami equation [34,35]

$$Z^*(\omega) = \frac{R_p}{[1+(j\omega\tau)^a]^b} \quad (2)$$

The shape parameters *a,b* lie in the range $0 < a,b \leq 1$.

As an example, the Cole impedance plot corresponding to TPU/2.8%-MWCNT composite, at several temperatures, are shown in Fig. 8. The plots are deformed arcs, roughly described by eq. (2), that intersect the abscissa axis at the extreme frequencies in such a way that $Z'(\infty) = 0$ and $Z'(0) = R_p$, being R_p the polarization resistance. The dc conductivity values were estimated from R_p values by means of the relationship $\sigma_{dc} = l/A \cdot R_p$. As we can observe in Fig. 6b, the dc conductivity values obtained are in reasonable good agreement with those obtained from the plateau in $\sigma' vs\ f$ plot.

Conclusions

This work is mainly focused on the study of the thermal and electrical properties of composites of TPU matrix loaded with different amounts of MWCNT.

The DSC analysis show the existence of two T_g associated with the soft and hard segment of TPU. While the T_g related to the hard segments is not affected significantly by the MWCNT content, the T_g associated with the soft segment decrease by increasing MWCNT content. That is, the MWCNT promotes the sliding of the molecular chains in the soft segment, bringing more disorder in these areas and decreasing T_g. Probably, the MWCNT not penetrant the hard segments and their T_g is unaffected.

The DRS was employed to study the MWCNT content effect on the conductivity behavior. The presence of MWCNT produces an enhancement of charge carriers trapping, increasing the electrical conductivity. These measurements show that the dielectric permittivity and electrical conductivity of the composites increase with the addition of MWCNT. Thus, an abrupt variation of both functions, related to the insulator to conductor transition, is observed at MWVNT content above 6wt%. The lower activation energy values observed for the high MWCNT contents can be rationalized if we consider that the mean distance between MWCNT decreases with increasing MWCNT content. The activation energy values obtained by the different procedures are in good agreement.

Acknowledgements

MJS and MC acknowledge the financial support of the DGCYT through Grant MAT2015-63955-R.

REFERENCES

[1] D.W. Schaefer, R.S. Justice, Macromolecules **40 (24)**, 8501-8517 (2007).

[2] D.R. Raul, L.M. Robeson, Polymer **49(15)**, 3187-3204 (2008).

[3] P.J. Brigandi, J.M. Cogen, R.A. Pearson, Polymer Engineering & Science **54 (1)**, 1-16 (2014).

[4] H. Deng, L. Lin, M. Ji, S. Zhang, M. Yang, Q. Fu, Progress in Polymer Science **39 (4)**, 627-655 (2014).

[5] R. Kumar, *Polymer-Matrix Composites. Types, Applications and Performance* (Nova Science Publishers, New York, 2014).

[6] Z. Wenying, Y. Demei, Journal of Applied Polymer Science **118(6)**, 3156–3166 (2010).

[7] Y.P. Mamunya, V.V. Davydenko, P. Pissis, E.V. Lebedev, European Polymer Journal **38(9)**, 1887–1897 (2002)

[8] B. Redondo-Foj, P. Ortiz-Serna, M. Carsí, M.J. Sanchis, M. Culebras, C.M. Gómez, A. Cantarero, Polymer International **64**, 284-292 (2015).

[9] S. Deng, Y. Zhu, X. Qi, W. Yu, F. Chen, Q. Fu, RSC Advances DOI:10.1039/C6RA09521F (2016).

[10] M. Khissi, M. El Hasnaoui, J. Belattar, M.P.F. Graça, M.E. Achour, L.C. Costa, J. Mater. Environ. Sci. **2(3)**, 281-284 (2011).

[11] M. Hindermann-Bischoff, F. Ehrburger-Dolle, Carbon **39(3)**, 375–382 (2001).

[12] I. Balberg, Carbon **40(2)**,139–143 (2002).

[13] M. Moniruzzaman, K.I. Winey, Macromolecules **39**,5194-5205 (2006).

[14] A. Bharati, R. Cardinaels, J.W. Seo, M. Wübbenhorst, P. Moldenaers, Polymer **79(19)**, 271-282 (2015)

[15] M. Szycher, *Handbook of Polyurethanes* (CRC Press:Washington DC,1999).

[16] C. Prisacariu, *Polyurethane Elastomers. From Morphology to Mechanical Aspects* (Springer:New York, 2011).

[17] P. Król, Prog. Mater. Sci. **52(6)**, 915-1015 (2007).

[18] P.R. de C Coelho Filho, M.S. Marchesin, A.R. Morales, J.R. Bartoli, Materials Research. **17(1)**, 127-132 (2014).

[19] R.H. Baughman, A.A. Zakhidov, W.A. de Heer, Science **297(5582)**,787-792 (2002).

[20] J. Kim, Y. Son Polymer **88**, 29-35 (2016)

[21] M.A. Nikje Mir, A. Yaghoubi, Polimery **59(11-12)**, 776-782 (2014).

[22] C. Kingston, R. Zepp, A. Andrady, D. Boverho, R. Fehir, D. Hawkins, J. Roberts, P. Sayre, B. Shelton, Y. Sultan, V. Vejins, W. Wohlleben, Carbon **68**, 33 –57 (2014).

[23] N.G. McCrum, B.E. Read, G. Williams, *Anelastic and Dielectric Effects in Polymeric Solids* (Wiley:London, 1967).

[24] F. Kremer, A. Schönhals, *In Broadband Dielectric Spectroscopy* (Springer:Berlin, 2003).

[25] E. Riande, R. Díaz-Calleja, *Electrical Properties of Polymers* (Dekker:New York,2004).

[26] I.M. Hodge, K.L. Ngai, C.T. Moynihan, J. Non-Crystalline Solids **351(2)**, 104-115 (2005).

[27] Eceiza, M.D. Martin, K. de la Caba, G. Kortaberria, N. Gabilondo, M.A. Corcuera, I. Mondragon, Polymer Engineering & Science **48(2)**, 297-306 (2008)

[28] A.K. Jonscher,*Universal relaxation law:a sequel to dielectric relaxation in solids* (Chelsea Dielectrics Press, Chapter 5, 1996)

[29] A.K. Jonscher, Nature **267**, 673-679 (1977).

[30] G. Li, L. Feng, P. Tong, Z. Zhai, Progress in Organic Coating **90**, 284-290 (2016)

[31] K.Petrie, M. Kontopoulou, A, Docoslis, Polymer Composites, **37(9)**, 2794-2802 (2016)

[32] N. Aranburu, J.I. Eguiazábal, Polymer Composites, **35(3)**, 587-595 (2014)

[33] E. Barsoukov, J.R. Macdonals, *Impedance Spectroscopy. Theory, Experiment, and Applications* (Wiley Interscience:New York, 2005).

[34] S. Havriliak, S.J. Havriliak *Dielectric and Mechanical Relaxation in Materials* (Hanser:Munich, Germany, 1997), p 57.

[35] S. Havriliak, S. Negami, Polymer **8(4)**, 161-210 (1967).

Table Captions

Table 1 DSC characteristic parameters of the TPU/*x*-MWCNT composites

Table 2 Parameters of the linear fit of the frequency dependence of the loss permittivity at 140ºC in the low frequency range.

Table 3 Conductivity activation energy and pre-exponential factor obtained by multiple regressions linear of the ln f_{max} of M'' dependence with reciprocal of temperature and the conductivity activation energy and pre-factor parameters obtained by multiple regressions linear of the ln σ_{dc} dependence with reciprocal of temperature (with σ_{dc} evaluated from the low frequency plateau and using the relationship $\sigma_{dc} = l/A \cdot R_p$).

Figure Captions

Fig. 1 Scheme of the chemical structure of TPU (Methylene diphenyl diisocyanate (MDI))

Fig. 2. FESEM micrographs of the TPU/*x*-MWCNT nanocomposites obtained from Zeiss Ultra In-lens detector at 5 kV with a WD of 4 mm (a: *x*=2.8, b: *x*=3.7, c: *x*=5.2 and d: *x*=10) and at 1kV with a WD of 3.3mm (e: *x*=6).

Fig. 3 DSC thermograms for TPU/*x*-MWCNT samples. [Curves: 1, *x*=0; 2, *x*=2.8; 3, *x*=3.7; 4, *x*=5.2; 5, *x*=6 and 6, *x*=10]. Data are vertically shifted for a better visualization. Only the cooling curve of sample 1 has been shown for clarity.

Fig. 4 Frequency dependence of the real and imaginary component of the complex permittivity at 120ºC for TPU/*x*-MWCNT samples (*x*=0, 2.8, 3.7, 5.2, 6 and 10 *%wt*). [Curves: 1, *x*=0; 2, *x*=2.8; 3, *x*=3.7; 4, *x*=5.2; 5, *x*=6 and 6, *x*=10]

Fig. 5 Frequency dependence of the imaginary component of the complex dielectric modulus at (a) 60ºC (open symbols) and (b) 120ºC (full symbols) for TPU/*x*-MWCNT samples (*x*=0, 2.8, 3.7, 5.2, 6 and 10 *%wt*). [Curves: 1, *x*=0; 2, *x*=2.8; 3, *x*=3.7; 4, *x*=5.2; 5, *x*=6 and 6, *x*=10]

Fig. 6 (a) Arrhenius plot obtained from the temperature dependence of $f_{\max}$ of M'' for TPU/*x*-MWCNT samples (*x*=0, 2.8, 3.7 and 5.2 *%wt*). (b) Temperature dependence of the dc conductivity evaluated from the low frequency plateau (open symbols) and using the relationship $\sigma_{dc} = l / A \cdot R_p$ (haft-filled symbols). [Curves: 1, *x*=0; 2, *x*=2.8; 3, *x*=3.7; 4, *x*=5.2; 5, *x*=6 and 6, *x*=10]

Fig. 7 Frequency dependence of the ac conductivity at 120ºC for TPU/*x*-MWCNT samples (*x*=0, 2.8, 3.7, 5.2, 6 and 10 *%wt*). Inset: MWCNT content dependence of the conductivity for TPU/*x*-MWCNT composites at 40º, 80º and 120ºC at 10^0 Hz. [Curves: 1, *x*=0; 2, *x*=2.8; 3, *x*=3.7; 4, *x*=5.2; 5, *x*=6 and 6, *x*=10]

Fig. 8 Cole-Cole impedance plots, at several temperatures for TPU/2.8%-MWCNT composite.

Table 1.

		T_g (soft segment)			T_g(hard segment)		
Sample	**MWCNT content (*%wt*)**	**ΔT (°C)**	**T_g(°C)**	**Δc_p(J/g°C)**	**ΔT (°C)**	**T_g(°C)**	**Δc_p(J/g°C)**
TPU	0	9.9	-15.5	0.470	10.3	79.2	0.191
TPU/*2.8*MWCNT	2.8	10.0	-16.3	0.477	9.0	78.9	0.149
TPU/*3.7*-MWCNT	3.7	9.2	-16.3	0.434	14.1	78.5	0.212
TPU/*5.2*-MWCNT	5.2	10.0	-16.3	0.433	15.1	78.6	0.238
TPU/*6*-MWCNT	6.0	11.1	-16.8	0.422	17.9	78.8	0.268
TPU/*10*-MWCNT	10.0	15.6	-19.4	0.429	19.4	78.9	0.243

Table 2

Sample	$log_{10}(\sigma/\varepsilon_0)$	***s***	σ ***(S/m)***
TPU	5.908±0.005	-0.984±0.002	$7.16 \cdot 10^{-6}$
TPU/*2.8*-MWCNT	5.919±0.008	-0.973±0.003	$7.35 \cdot 10^{-6}$
TPU/*3.7*-MWCNT	8.698±0.009	-1.003±0.002	$4.42 \cdot 10^{-3}$
TPU/*5.2*-MWCNT	9.199±0.011	-1.002±0.003	$1.40 \cdot 10^{-2}$
TPU/*6*-MWCNT	10.350±0.002	$-1.008 \pm 5.792 \cdot 10^{-4}$	$1.98 \cdot 10^{-1}$
TPU/*10*-MWCNT	12.436±0.006	-1.016±0.002	$2.42 \cdot 10^{1}$

Table 3

	from M'' *vs* f		**from plateau σ' *vs* f**		**by using $\sigma_{dc} = l/A \cdot R_p$.**	
Sample	**ln f_0**	***E_a (kJ/mol)***	**ln σ_0 (S/m)**	***E_a (kJ/mol)***	**ln σ_0 (S/m)**	***E_a (kJ/mol)***
TPU	31.2±0.4	72.7±1.2	8.67±0.32	72.7±0.9	–	–
TPU/*2.8*-MWCNT	27.9±0.1	65.3±0.3	6.19±0.27	65.3±0.8	6.60±0.46	66.6±1.4
TPU/*3.7*-MWCNT	28.0±0.2	64.3±0.6	6.18±0.20	64.3±0.6	6.08±0.26	64.5±0.8
TPU/*5.2*-MWCNT	27.7±0.2	64.0±0.5	6.50±0.34	64.0±0.9	6.34±0.33	63.8±1.0
TPU/*6*-MWCNT			6.06±0.24	62.1±0.7	5.84±0.52	61.2±1.5
TPU/*10*- MWCNT			19.74±0.17	61.2±0.5	–	–

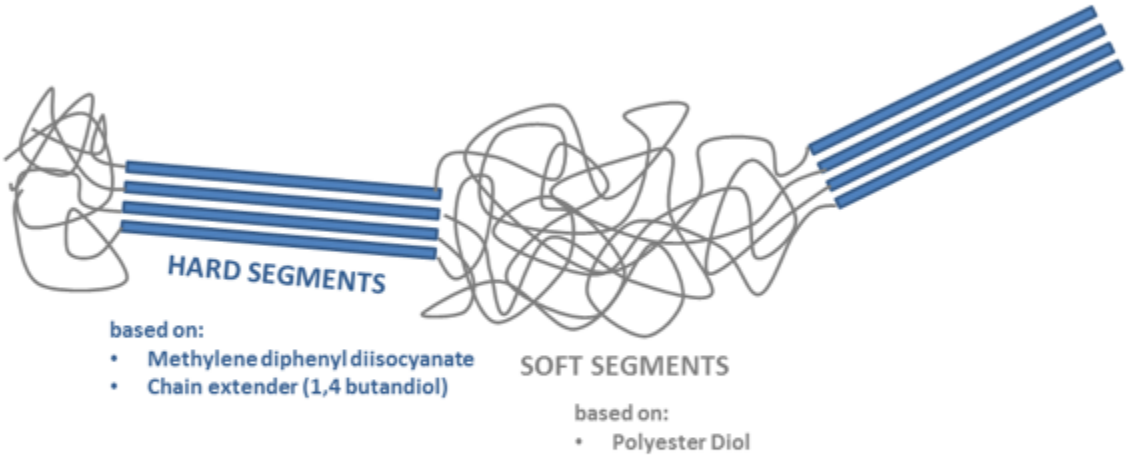
HARD SEGMENTS
based on:
• Methylene diphenyl diisocyanate
• Chain extender (1,4 butandiol)
SOFT SEGMENTS
based on:
• Polyester Diol

Fig1

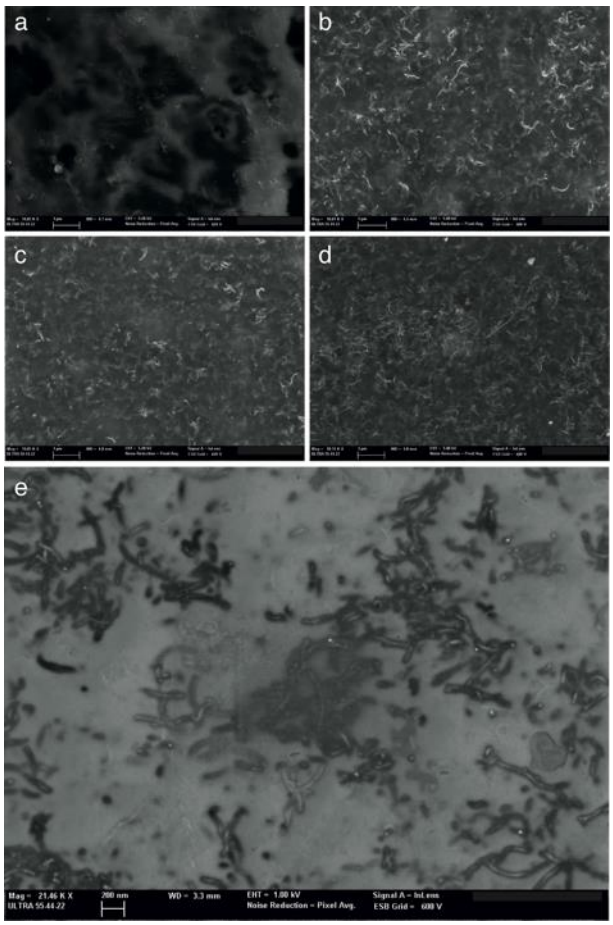
a
b
c
d
e
Mag = 21.46 K X
ULTRA 55-44-22
200 nm
WD = 3.3 mm
EHT = 1.00 kV
Noise Reduction = Pixel Avg.
Signal A = InLens
ESB Grid = 688 V

Fig 2

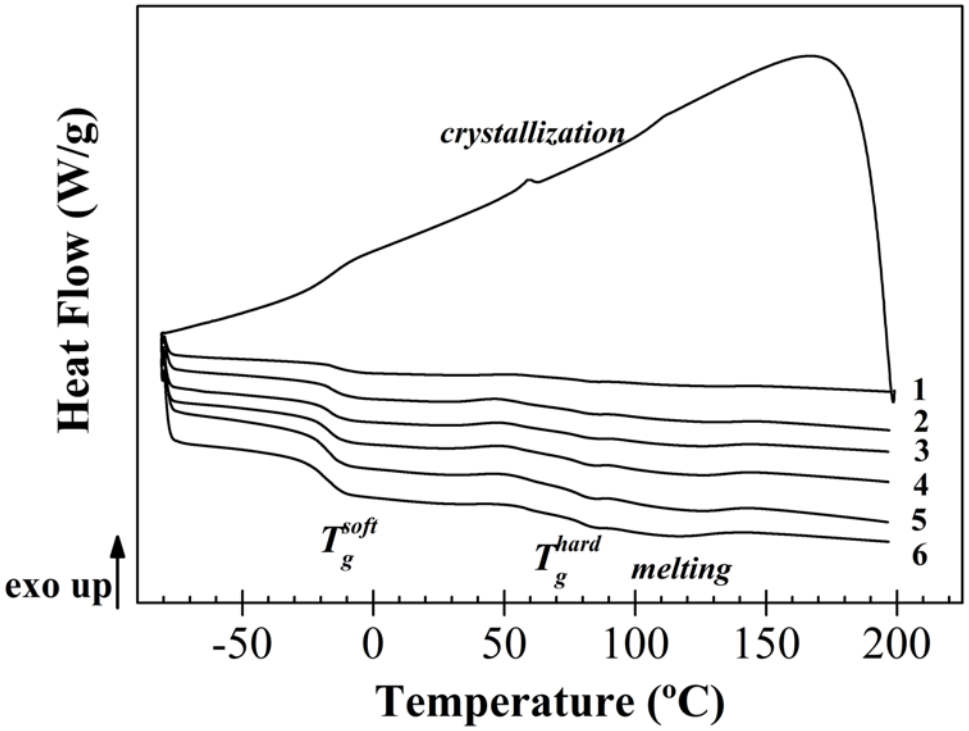
Heat Flow (W/g)
crystallization
1
2
3
4
5
6
T_g^{soft}
T_g^{hard}
melting
exo up
-50
0
50
100
150
200
Temperature (ºC)

Fig 3

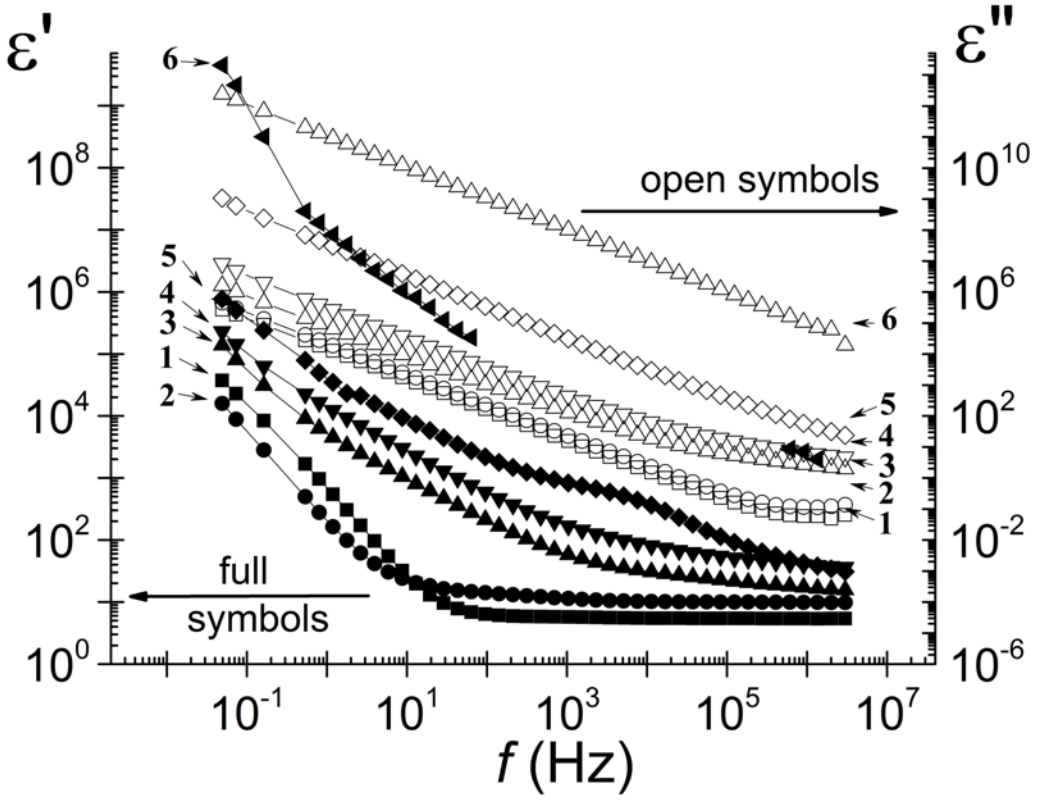
ε'
ε"
open symbols
full
symbols
f (Hz)
10^8
10^6
10^4
10^2
10^0
10^10
10^6
10^2
10^-2
10^-6
10^-1
10^1
10^3
10^5
10^7
1
2
3
4
5
6

Fig 4

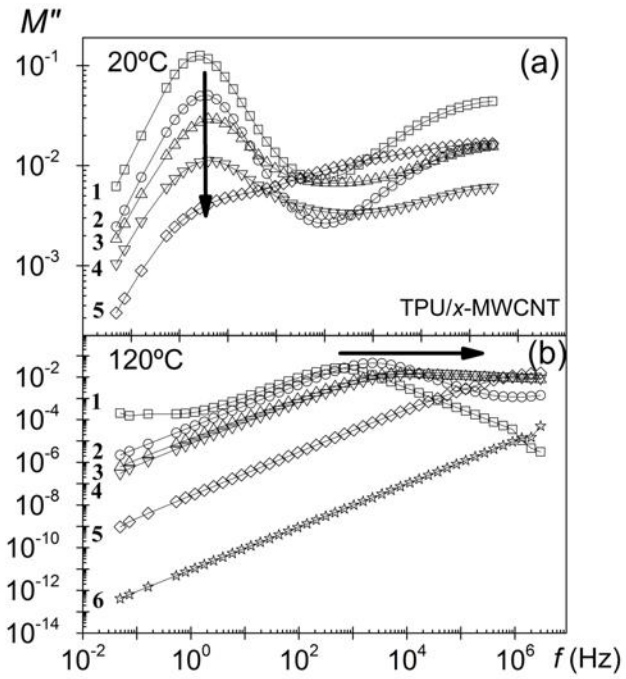

Fig 5

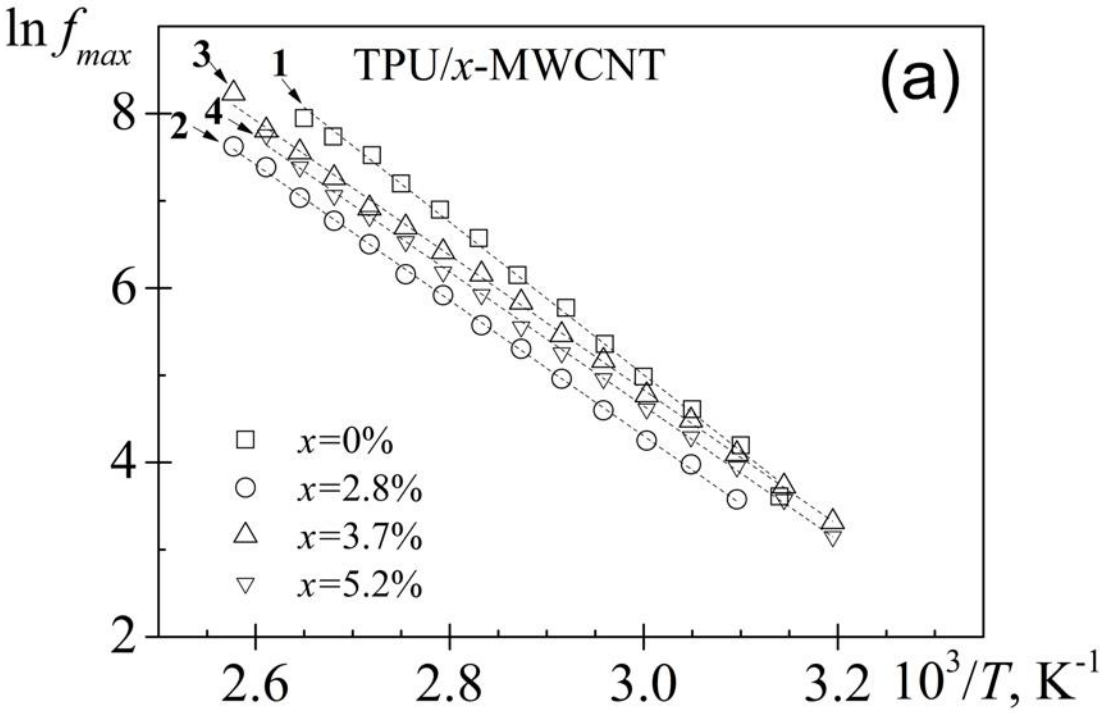
ln f_{max}
TPU/x-MWCNT
(a)
1
2
3
4
8
6
4
2
x=0%
x=2.8%
x=3.7%
x=5.2%
2.6
2.8
3.0
3.2
$10^3/T$, K^{-1}

Fig. 6a

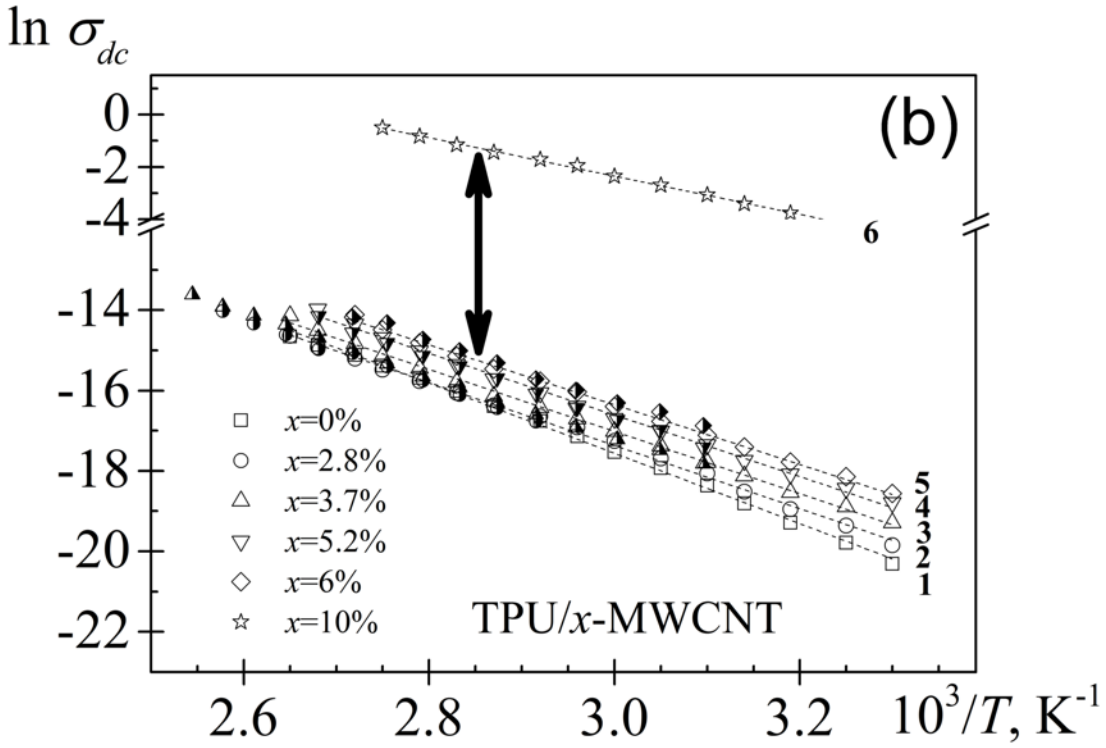
ln σ_{dc}
(b)
0
-2
-4
-14
-16
-18
-20
-22
6
5
4
3
2
1
x=0%
x=2.8%
x=3.7%
x=5.2%
x=6%
x=10%
TPU/x-MWCNT
2.6
2.8
3.0
3.2
$10^3/T$, K^{-1}

Fig. 6b

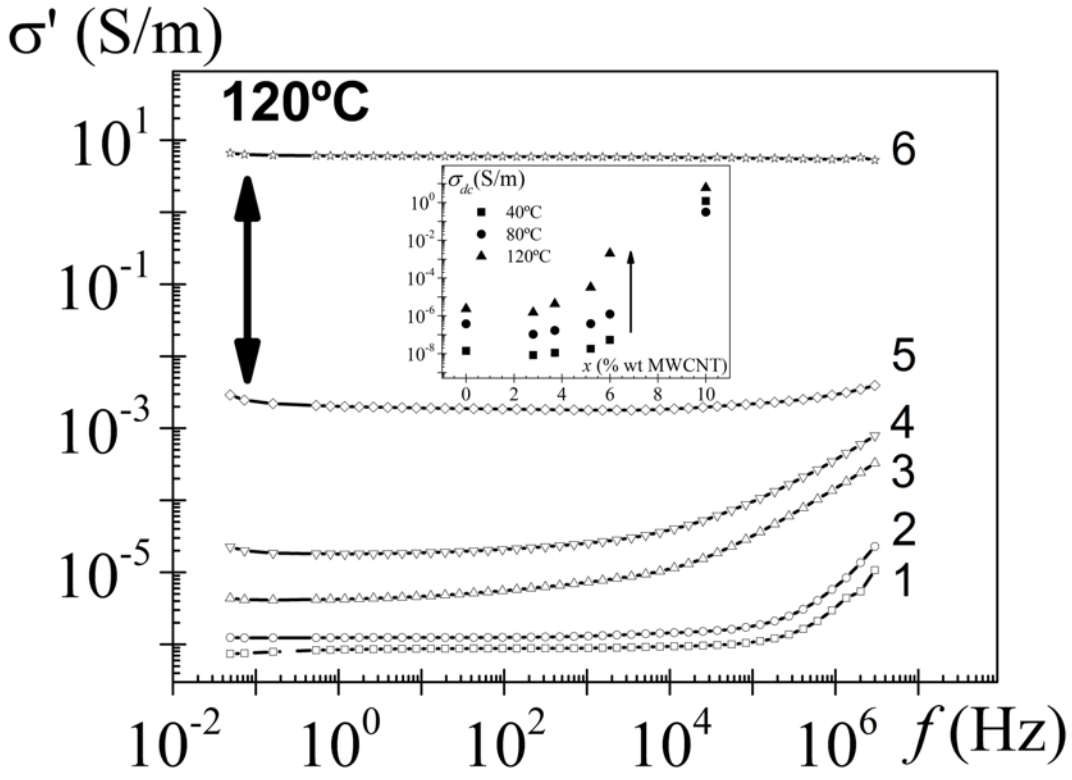
σ' (S/m)
120ºC
10^{1}
10^{-1}
10^{-3}
10^{-5}
10^{-2}
10^{0}
10^{2}
10^{4}
10^{6}
f (Hz)
6
5
4
3
2
1
σ_{dc}(S/m)
40ºC
80ºC
120ºC
x (% wt MWCNT)

Fig. 7

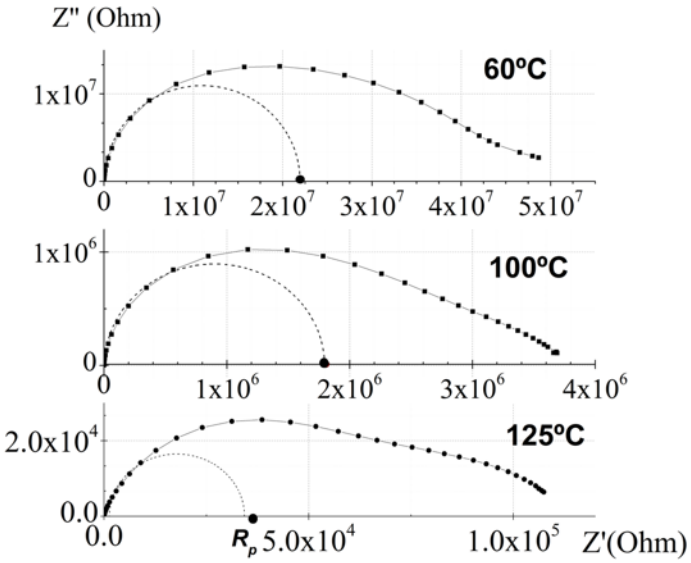
Z" (Ohm)
60ºC
1x10^7
0
0
1x10^7
2x10^7
3x10^7
4x10^7
5x10^7
1x10^6
100ºC
0
0
1x10^6
2x10^6
3x10^6
4x10^6
2.0x10^4
125ºC
0.0
0.0
R_p 5.0x10^4
1.0x10^5
Z'(Ohm)

Fig. 8

Graphical Abstract

Thermal and Dielectric Characterization of Multi-walled carbon nanotubes (MWCNTs)-Thermoplastic polyurethanes (TPU) Composites

M. J. Sanchis[a*], M. Carsí[a,b], C. A. Gracia-Fernández[c]

[a]*Departamento de Termodinámica Aplicada, E.T.S.I.I., Instituto de Tecnología Eléctrica Universitat Politècnica de Valencia, 46022 Valencia, Spain*

[b]*Instituto de Automática e Informática Industrial, Universitat Politècnica de Valencia, 46022 Valencia, Spain*

[c]*TA Instruments-Waters Cromatografía, 20108 Alcobendas, Madrid, Spain*